



Insight into heat transfer process of graphene aerogel composite phase change material

Ping Yang ^a, Bo Wu ^b, Xuan Tong ^c, Min Zeng ^a, Qiuwang Wang ^a, Zhilong Cheng ^{a,*}

^a Key Laboratory of Thermo-Fluid Science and Engineering, Ministry of Education, Xi'an Jiaotong University, Xi'an, 710049, China

^b AVIC Xi'an Aeronautics Computing Technique Research Institute, Xi'an, 710068, China

^c Shanghai Nuclear Engineering Research and Design Institute, Shanghai, 200030, China

ARTICLE INFO

Handling Editor: Neven Duic

Keywords:

Graphene aerogel
Composite phase change material
Heat transfer improvement
Thermal management
Cascade arrangement

ABSTRACT

With electronic device miniaturization and integration, its thermal management is encountering challenges of high heat flux and eliminating thermal stress. Phase change thermal control is paid more attention to due to its high energy density and temperature uniformity. Therefore, a visual experimental platform was established to investigate the heat transfer and phase change characteristics of graphene aerogel composite phase change materials in this study. The results indicate that the heat dissipation enhancement of those composite materials can reach 220.8%, while graphene aerogel has the opposite effects of heat conduction enhancement and convection suppression. Furthermore, two new cascade arrangements are proposed and the effects of cascade arrangements on heat transfer performance are discussed. The improvement effect is best when the thermal conductivity increases longitude from top to bottom, whose heat dissipation efficiency is 207.5%, which is 11% higher than that of the group without cascade configurations. The horizontal cascade arrangement proposed in this study achieves an effective combination of heat conduction enhancement and convection heat transfer. Its heat dissipation is 12% more effective than the cavity filled with pure CPMCs using the same amount of porous materials, and the phase change speed is increased by 149 s.

1. Introduction

With the electronic device miniaturization and integration, its heat dissipation faces the issues of high heat flux, non-uniform temperature and space constraint [1]. According to statistics, more than 55% of electronic equipment failures are caused by temperature control ineffectiveness [2]. Phase change thermal management is paid more attention to due to its high energy density and nearly constant phase change temperature [3]. Therefore, it is extremely necessary to investigate the heat transfer characteristics of phase change materials (PCMs).

Although there is a wide variety of organic PCMs, low thermal conductivity is their common inherent drawback [4]. Generally, using high thermal conductivity materials [5], disrupting boundary layer, fluidization [6] and reducing contact thermal resistance [7] are common heat transfer enhancement methods. Inserting high thermal conductivity fins and adding high conductivity particles are more suitable for PCMs applications [5]. Metal fins [8] and foams [9] are used to improve thermal conductivity and can encapsulate PCMs to prevent leakage, while high metal proportions will result in latent heat loss significantly.

Nano-metal particles [10], graphite powder [11] and carbon nanotubes [12] are popular particles of high conductivity to enhance the PCM thermophysical properties. However, the particles may precipitate in the PCMs due to gravity after a few melting and solidification cycles, reducing their service life. On the other hand, the dispersed high thermal conductivity particles could not avoid the leakage of liquid phase change materials. To combine the advantages of the above two enhancement methods, some researchers proposed constructing shape-stabilized skeletons using high thermal conductivity nanomaterials. As confirmed by the literature [13], nanoporous composite phase change materials (CPCMs) such as graphene CPCMs can overcome low thermal conductivity, leakage and supercooling, but their preparation and practical application are still a great challenge.

Graphene is a single layer of carbon atoms arranged in a hexagonal lattice, and graphene aerogel is a three-dimensional (3D) carbon-based material formed by graphene. Shang and Zhang [14] proposed a one-pot method to synthesize 3D graphene aerogel networks and pointed out that this method was more convenient and controlled because the impregnation and freeze-drying can be neglected compared to other methods. Liao et al. [15] explored a way to prepare a lightweight and

* Corresponding author.

E-mail address: chengzl@xjtu.edu.cn (Z. Cheng).

Nomenclature	
A	heat transfer area (m^2)
L	length (m)
P	thermal power (W)
Q_n	net heat dissipation (J)
Q_{n-c}	net heat dissipation of the composite material groups (J)
Q_{n-b}	net heat dissipation of the paraffin group (J)
q	heat flux ($\text{W}\cdot\text{m}^{-2}$)
Δq	net heat flux ($\text{W}\cdot\text{m}^{-2}$)
T	temperature ($^\circ\text{C}$)
t	time (s)
<i>Greek symbols</i>	
η	heat dissipation enhancement efficiency (%)
λ	thermal conductivity ($\text{W}\cdot\text{m}^{-1}\cdot\text{K}^{-1}$)
<i>Abbreviations</i>	
CPCM	composite phase change material
DC	direct current
EDA	anhydrous ethylenediamine
GNP	graphene nanosheet
GO	graphene oxide
PCM	phase change material
PMMA	polymethyl methacrylate
PW	paraffin wax

mechanically strong 3D graphene aerogel, which could withstand high mechanical strength up to 66.7 kPa. Wu et al. [16] summarized the common synthesis methods of three-dimensional graphene aerogels in recent years. They concluded that in addition to the template-assisted method, the self-assembly method and the 3D printing method, thermal/electrochemical expansion, centrifugal evaporation-induced methods and electrochemical reduction are conspicuous novel approaches. Moreover, except for the graphene aerogel synthesis, the research on the property characteristics of various CPCMs prepared are also the focus. Bai et al. [17] prepared ionic liquid composite materials with excellent thermal stability using graphene for battery thermal management, and they illustrated the interactions between ionic liquid matrices and graphene. Wang et al. [18] reported a solar-driven graphene CPCM and systematically measured its full-spectrum absorption capacity and thermal storage performance. The results showed that the optical absorption capacity and photo-thermal conversion efficiency of the best composite material in their study are 79.12% and 69.73%, respectively. Similarly, Luo et al. [19] used gallic acid-modified graphene nanosheets (GNPs) and pentaerythritol to synthesize composite materials for solar energy, of which the photothermal conversion efficiency was 93.86% when the CPCMs contained 15 wt% GNPs. However, those investigations of graphene aerogel CPCMs are mostly focused on the physical properties characterization, and rarely on practical application characteristics.

Except for studying the physical characterization of the graphene nano-PCMs, Sathishkumar and Cheraiyathan [20] clarified the charging and discharging processes of the small cool thermal energy storage tank when the inlet temperature and volumetric flow rate of the heat transfer fluid were different. Arici et al. [21] integrated the PCMs into the external building walls to reduce energy consumption. They compared the thermal performance between walls with PCMs and walls with Phase Stabilized PCMs, which have the same thermal properties as PCMs except for phase change, to reveal the improvement mechanism due to the latent heat. Zhang et al. [22] embedded expanded graphite CPCMs in the printed circuit heat exchanger to suppress temperature fluctuations

Table 1
Major materials used in the present study.

Materials	properties
GO	Purity > 97 wt%, Number of layers < 5, Thickness: 0.55–2 nm , Size: 3–10 μm
GNPs	Purity > 99.5 wt%, Number of layers < 20, Thickness: 4–20 nm , Size: 5–10 μm
Paraffin	48–50 $^\circ\text{C}$
Anhydrous ethanol	Content \geq 99.7%
EDA	Content \geq 99.0%

in the supercritical CO₂ cycle. The numerical results showed that a reasonable arrangement of CPCMs can reduce the temperature fluctuations on the hot and cold sides by 22.37% and 38.16%. Chen et al. [23] represented the thermal control characteristics of CPCMs in the lithium battery module and found that the temperature difference can be controlled within 5 $^\circ\text{C}$. However, those studies focused on the optimization effects due to the PCMs application, like the temperature fluctuation decrease in the supercritical CO₂ cycle or the temperature difference in battery modules. The heat transfer process inside PCMs didn't be illustrated in detail. In the practical application of PCMs, cascade arrangement is widely used due to its high efficiency. Park et al. [24] designed a cascade energy storage system with PCMs of three different melting points and used an intelligent control method to change the input position of heat transfer fluid under unsteady temperature conditions. Wang et al. [25] prepared a graphene oxide (GO) hybrid aerogel CPCM with gradient freezing points and tested its thermal insulation performance of the battery in a cold environment. EL-Sihy et al. [26] established a numerically concentric model of cascade latent heat packed-bed, and revealed cyclic dynamic characteristics of cascade structure. Christopher et al. [27] reviewed mathematical studies of the optimal melting temperature in each layer PCMs and summarized factors affecting thermal performance of cascade configurations such as stage numbers.

From the literature review, the previous studies of graphene aerogel CPCMs rarely reflected the heat transfer process. However, investigations on heat transfer characteristics of CPCMs are the basis for PCMs application. Moreover, the cascade arrangements in the general application were mainly based on different phase change temperatures, which could not fully utilize the advantages of graphene. The phase change temperature of organic PCMs is also difficult to be controlled precisely. Therefore, a visual experimental platform was established to investigate the heat transfer process of graphene aerogel CPCMs in this study. Based on heat transfer characteristics, two new cascade arrangements are performed to coordinate the internal heat transfer of CPCMs and improve the heat transfer effect. The results of this study pave the foundation for the thermal management of graphene CPCMs and provide a new idea for heat transfer improvement.

2. Materials and methods

Material preparation (Section 2.1) and experimental information (Section 2.2) are introduced in this part. Moreover, the experimental information includes experimental platform composition (Section 2.2.1) and experimental method introduction (Section 2.2.2).

2.1. Material preparation

According to our previous results [28], the hydrothermal self-assembly method was used to synthesize graphene aerogel. The main materials used for preparing the graphene aerogel CPCMs are shown in Table 1. GO and GNPs were mixed at the mass ratio of 1:1 as mixed powders to prepare graphene aerogel. Anhydrous ethylenediamine (EDA) as a reducing agent was added to increase the reduction degree of GO [29], which improved the thermal conductivity of

Table 2

Necessary information of four graphene aerogel CPCMs.

	Pure paraffin	PW-GO-1	PW-GO/GNP-1	PW-GO/GNP-2	PW-GO/GNP-3
Mixed powder mass ratio	–	GO: GNP = 1:0	GO: GNP = 1:1	GO: GNP = 1:1	GO: GNP = 1:1
GO or GO/GNPs solution mass ratio	–	1:100	1:100	2:100	3:100
Thermal conductivity ($\text{W}\cdot\text{m}^{-1}\cdot\text{K}^{-1}$)	0.2073	0.2365	0.2911	0.3428	0.4347
Latent heat ($\text{J}\cdot\text{g}^{-1}$)	209.86	200.70	183.60	192.07	183.00
Specific heat ($\text{J}\cdot\text{kg}^{-1}\cdot\text{K}^{-1}$)	2834	2754	2742	2680	2621
Density ($\text{g}\cdot\text{cm}^{-3}$)	0.881	0.923	0.948	0.969	0.999
Graphene mass fraction	–	1.66%	2.01%	3.35%	4.40%

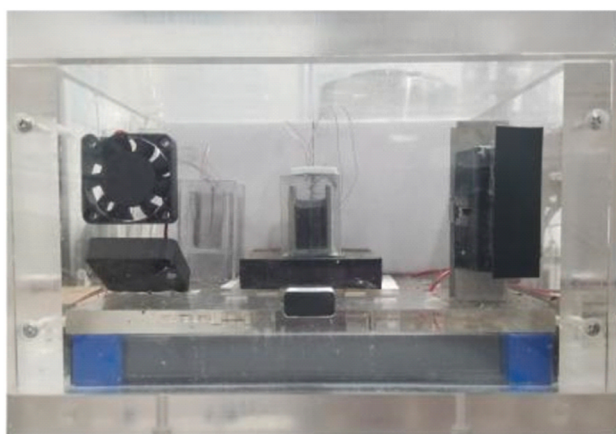


Fig. 1. Experimental platform photo.

graphene aerogel CPCMs.

The synthesis of graphene aerogel CPCMs tested in this study could be divided into four steps as follows:

- (1) Hydrothermal reaction: The predefined GO/GNPs mixed powders were dispersed in deionized water using ultrasonic with designed mass ratios. Then GO/GNPs solution and EDA solution were poured into a closed hydrothermal reactor before heating at a specific temperature (130–160 °C) for 1–3 h. The formed graphene hydrogel was obtained after cooling.
- (2) Dialysis: The graphene hydrogel was dialyzed in the low-concentration ethanol solution for 12–24 h.
- (3) Freeze drying: The graphene hydrogel was placed in a freeze dryer after dialyzing. It was frozen for 6 h at –50 °C and then vacuumed for 24–48 h with the vacuum degree below 10 Pa. Graphene aerogel was obtained after freeze drying.
- (4) Vacuum filling: The graphene aerogel was placed on the paraffin upper surface before heating together in a vacuum barrel. The vacuum was applied 10–15 min after the melting, and then the pressure was released to fill the paraffin due to the pressure difference.

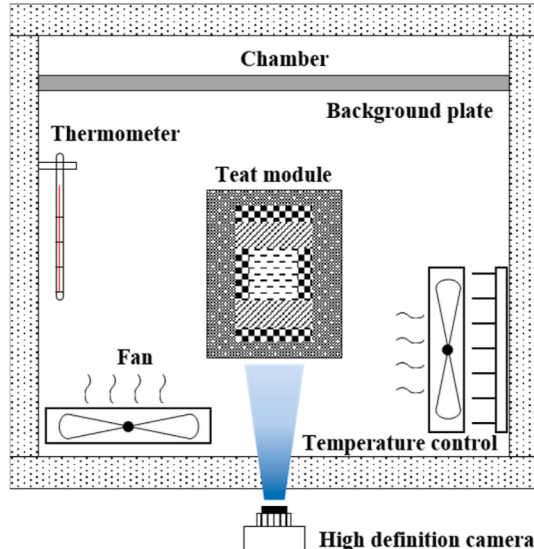
As shown in Table 2, four different graphene aerogel CPCMs were prepared by changing the GO/GNPs solution ratio in the hydrothermal reaction. More detailed preparation processes and physical characterization of CPCMs can refer to our previous investigations [28].

2.2. Experimental platform and methods

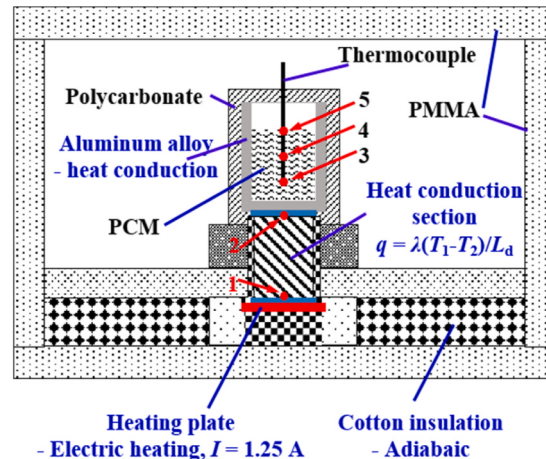
This section introduces the experimental platform and method in section 2.2.1 and section 2.2.2, respectively.

2.2.1. Experimental platform

The phase change experimental system included a direct current (DC) power supply, an experimental chamber, and a data acquisition unit. Fig. 1 is a physical picture of the experimental platform. The experimental chamber is the main body of this experimental system, of



(a) The internal schematic diagram of the experimental chamber



(b) The main structures of the test module

Fig. 2. Diagram of the experimental chamber

(a) The internal schematic diagram of the experimental chamber (b) The main structures of the test module.

Table 3
Measurement parameters errors.

Parameter	Error
Temperature	0–95 °C, ±0.1 °C
Length	±0.5%
Mass	±0.5%
Thermal conductivity	±1.6%
Data acquisition device	±0.01%

which the internal schematic diagram is presented in Fig. 2(a), including the temperature control module, test module, high-definition camera, fan and background board. The experimental chamber frame was made of polymethyl methacrylate (PMMA) for convenient observation. The background plate was used with a high-definition video camera to record the experimental process visually. Furthermore, the core component of the experimental chamber is the test module, whose main structures are shown in Fig. 2(b). A polyimide heating film was attached to the brass sheet as a heat source. A stainless steel block (length 30 mm, cross section 20 × 20 mm, thermal conductivity 14.13 W·m⁻¹·K⁻¹) was used as the heat conduction section connecting the heat source to the aluminum cavity. Thermally conductive silicone grease was used as the interface material to reduce contact thermal resistance.

The high thermal conductivity of aluminum alloy (2A12) can accelerate the heat conduction and phase change rate. Polycarbonate has great temperature resistance and transmission for visualization experiments. Therefore, the phase change cavity consisted of aluminum (2A12) and polycarbonate. The internal size of the phase change cavity was 18 × 18 × 35 mm. The thermocouple layout is shown in Fig. 2(b). Test Locations 1 and 2 were located at the centers of the lower and upper surfaces of the heat conducting section, so the temperature of Location 2 (T_2) can reflect the temperature control effect. Test Location 3 was located in the inner cavity center and 5 mm high from the bottom inner surface. Besides, the distance between Locations 4 and 3 was 10 mm, and between Locations 5 and 3 was 20 mm.

According to the manufacturer instruction, error analyses of the measuring parameters are shown in Table 3.

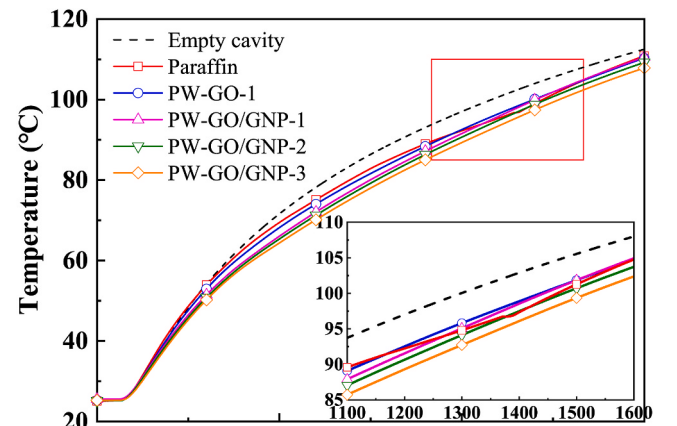
2.2.2. Experimental method

Firstly, the composite phase change material should be preheated at 47 °C for 20 min to soften, and then a square rod was used to push it into the square cavity, which made it completely adhere to the inner wall due to its deformation. After that, the experimental chamber temperature was initialized to 25.0–25.5 °C using the fan and temperature control module. Subsequently, the time and temperature recording were started. Experiments aim to investigate the heat dissipation capability of graphene CPCMs, so the melting phase change is the focus in this study. The heating and video recording were started at $t = 60$ s and stopped at $t = 1800$ s.

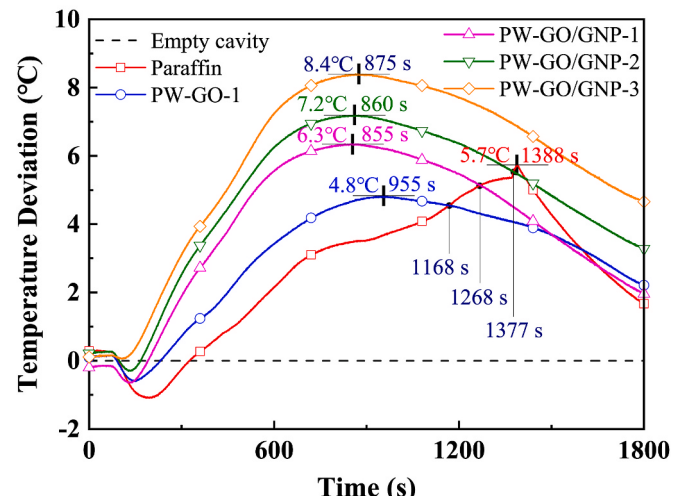
As shown in Fig. 2(b), temperatures T_1 and T_2 at the two ends of the heat conduction section can be used to calculate the thermal control capability of each experimental unit. The thermal conductivity of the ceramic fiber is only 0.08 W·m⁻¹·K⁻¹. Therefore, it is assumed that the heat conduction section is insulated and the temperature of each section is uniform. According to the Fourier heat conduction law, heat flux through the heat conduction section can be calculated as follows:

$$q = \lambda_d \frac{T_1 - T_2}{L_d} \quad (1)$$

where λ_d is the thermal conductivity (W·m⁻¹·K⁻¹), and L_d is the heat conduction section length (m). In this way, the heat flux transmitted to the phase change materials via the heat conduction section can be monitored. The heat transfer power P can also be obtained, $P = qA_d$, where A_d is the cross-section area of the heat conduction section (m²).



(a) Temperature comparison of Location 2



(b) Temperature deviation comparison

Fig. 3. Comparison of temperature variations in each experimental group.

3. Results and discussion

The heat transfer and phase change process of CPCMs prepared in section 2 are discussed in detail in this part. Two new cascade arrangements are proposed and their effects on heat transfer are investigated in this part.

3.1. Heat transfer characteristics of CPCMs

The heat transfer characteristics of graphene aerogel CPCMs during phase change are investigated in this section. There are six experimental groups as follows: (1) empty cavity; (2) pure paraffin (PW); (3) PW-GO-1; (4) PW-GO/GNP-1; (5) PW-GO/GNP-2; and (6) PW-GO/GNP-3. Groups (3)–(6) are graphene CPCMs prepared in section 2, as shown in Table 2.

3.1.1. Temperature change during the phase change

The thermal control characteristics can be analyzed through the temperature variation of T_2 . As shown in Fig. 3(a), T_2 of all CPCM groups were lower than that of the pure paraffin group and decreased with increasing GO/GNPs mass ratio in the initial heating stage. With phase transition proceeding, the temperature increase rate of the paraffin

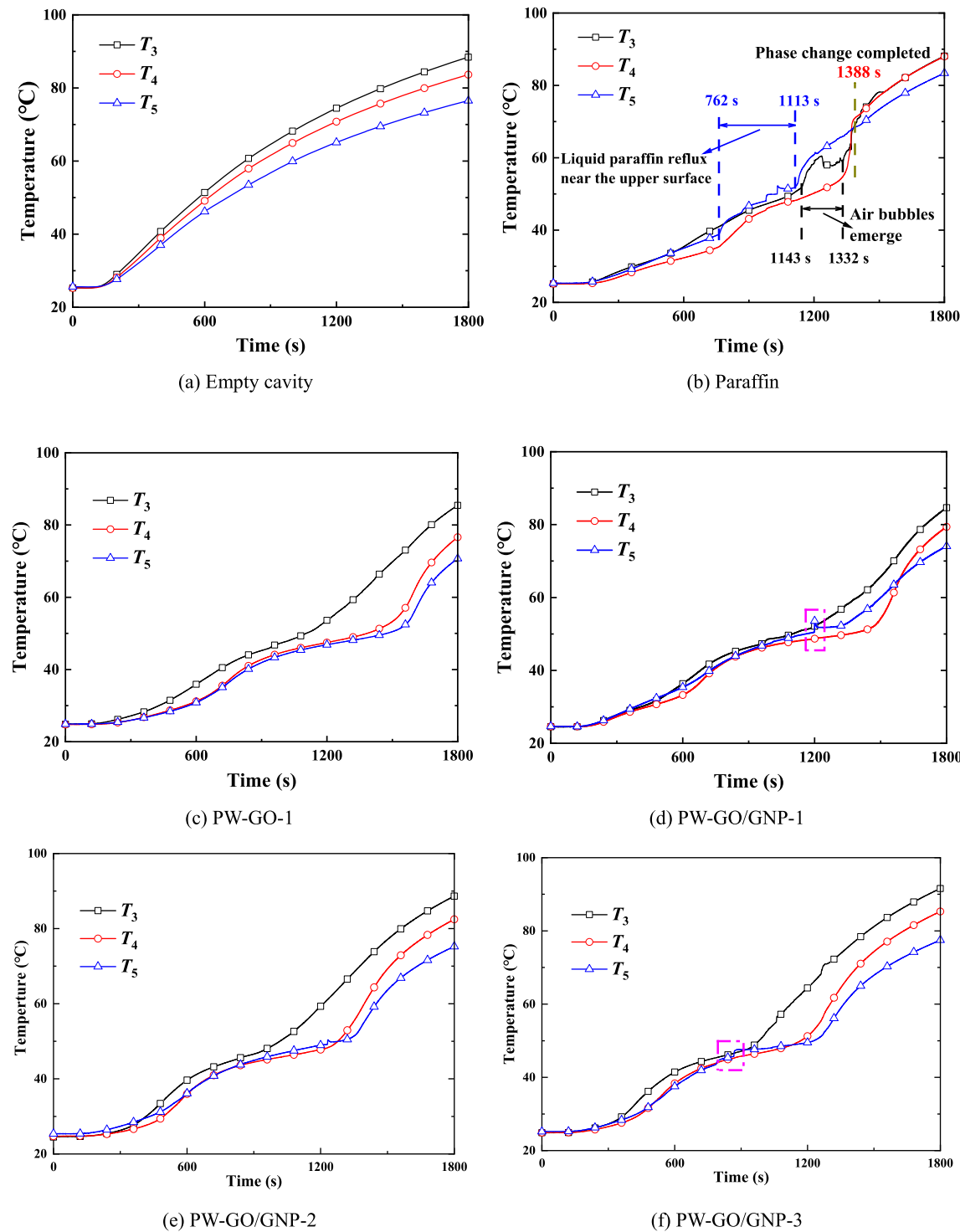
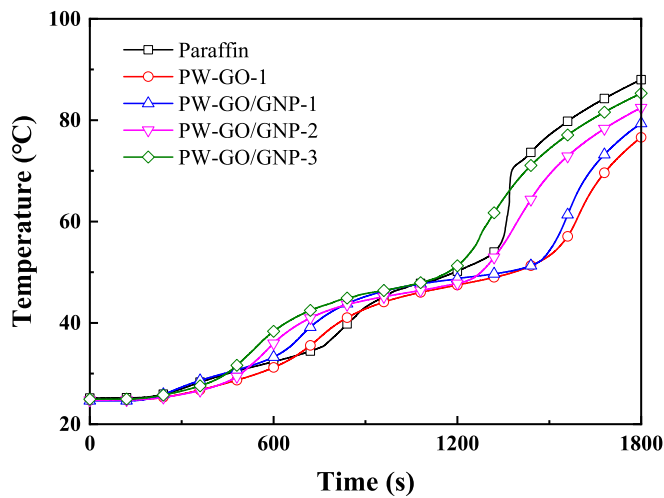
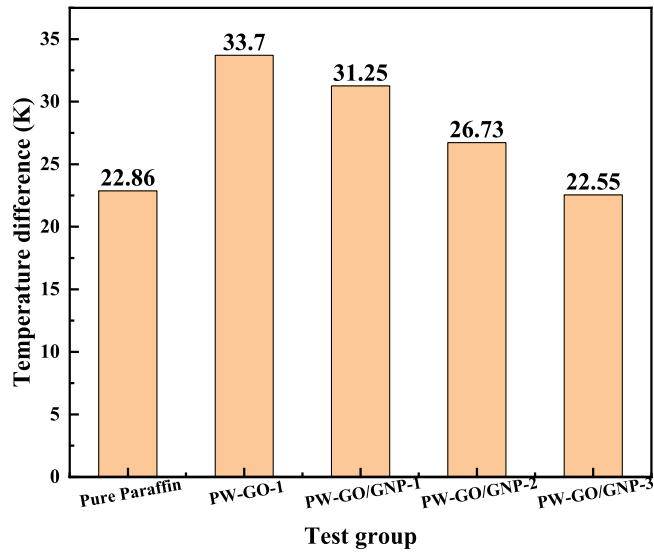


Fig. 4. Temperature variations of Locations in each experimental unit.

decreased, so there were intersection points with the curves of PW-GO-1, PW-GO/GNP-1 and PW-GO/GNP-2, while T_2 of PW-GO/GNP-3 was always lower than that of the paraffin due to its superior thermal conductivity. Moreover, Fig. 3(a) illustrates that T_2 of the cavity without PCMs was the highest temperature, which means filling PCMs can enhance temperature control. For quantitative analysis, the group without PCMs was used as a reference group, and the temperature difference of T_2 between other groups and the empty cavity was presented in Fig. 3(b). The peaks of groups PW-GO-1, PW-GO/GNP-1, PW-GO/GNP-2, and PW-GO/GNP-3 were located at $t = 955$ s, 855 s, 860 s,

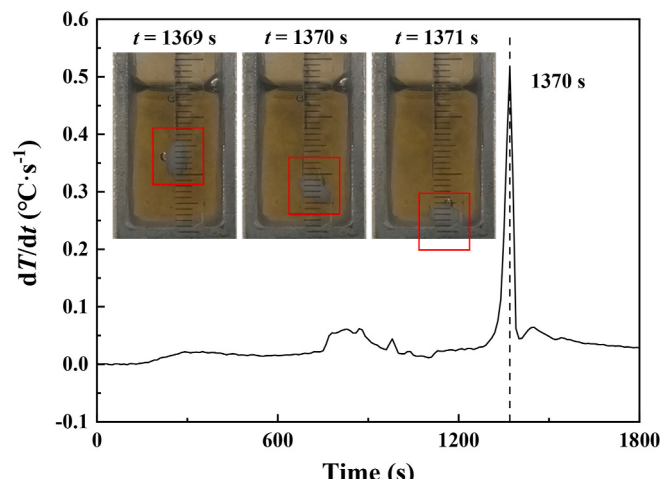
and 875 s. The maximum temperature differences with the empty cavity were 4.8 °C, 6.3 °C, 7.2 °C, and 8.4 °C, respectively, which were higher than those of the paraffin group at the same time. After reaching the peak value, the temperature control effect of CPCMs groups began to decrease, while that of the paraffin group was still increasing. The temperature difference of the paraffin group surpassed that of three CPCMs groups at $t = 1168$ s, 1268 s and 1377 s, and then reached the peak of 5.7 °C at $t = 1388$ s. Phase change, heat conduction and liquid convection of PCMs result in the highest T_2 in the empty cavity. However, the different thermal conductivity of CPCMs and the convection

(a) T_4 varies with time(b) Temperature difference $\Delta T = T_2 - T_4$ at $t = 1800$ s**Fig. 5.** T_4 and the temperature difference between PCMs and the heating wall $\Delta T = T_2 - T_4$ in each group.

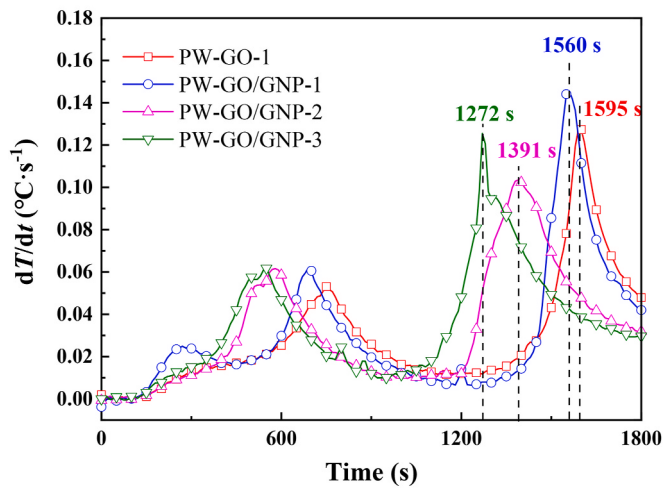
suppression effect of graphene make the heat dissipation enhancements efficiency different. More detailed information will be discussed in the following sections.

The phase change interface of CPCMs cannot be visually identified by photos such as pure paraffin. Internal heat transfer and phase change process are studied through temperature analysis of Locations 3–5 arranged inside the material. Fig. 4 shows the temperature variation of Locations inside each group with time. As shown in Fig. 4(a), temperatures in the cavity without PCMs rise smoothly because the heat was transferred to Locations 3–5 only through air convection. Fig. 4(b) shows that the T_3 and T_5 within paraffin fluctuate more due to phase interfacial propulsion, natural convection, and air bubbles emerging. The temperature variations of Locations 3–5 in each CPCM group are presented in Fig. 4(c)–4(f). Similar to pure paraffin, the temperature increase rate was slow during the initial heating and phase change but suddenly became faster after the phase transition. Moreover, paraffin volume expansion caused the liquid paraffin to seep upward, leading T_5 to be higher than T_3 at some time, as shown in Fig. 4(d).

In comparison, the temperature change at Location 4, closest to the center of the phase change material inside the cavity, can better reflect



(a) Paraffin



(b) Composite phase change materials

Fig. 6. Variations of T_4 temperature rise rate in each group.

the phase change process of different test units. Therefore, Fig. 5 compares T_4 and the temperature difference between PCMs and the heating wall $\Delta T = T_2 - T_4$ in each group. It can be seen that the temperature difference of paraffin at $t = 1800$ s isn't the maximum, which means the thermal resistance of pure paraffin isn't the maximum. At $t = 1800$ s, all melting phase change in each group is ending, so only convection and heat conduction affect the temperature difference $\Delta T = T_2 - T_4$. Pure paraffin has the lowest thermal conductivity, but its thermal resistance isn't the maximum after melting, which confirms the internal porous structure of CPCM has an inhibitory effect on convection. Moreover, T_4 of PW-GO/GNP-3 < T_4 of PW-GO/GNP-2 < T_4 of PW-GO/GNP-1 < T_4 of PW-GO-1 means heat conduction is still dominant in CPCMs after phase transition and improving the thermal conductivity of CPCMs can reduce the convection inhibition effect. Besides, the phase transition time of PW-GO-1 and PW-GO/GNP-1 maybe be longer than that of paraffin because the dramatic change of T_4 is later.

To further investigate the phase change rate of the graphene CPCMs, the temperature increase rate variations in each group are shown in Fig. 6. Fig. 6(a) shows that the peak value of the temperature increase rate is at $t = 1370$ s. Compared with recorded photos, the last small piece of solid paraffin in the cavity separated from Location 4 and sank to the bottom at this time. As a result, the remaining paraffin blocks could not be attached and settled, which caused an abrupt change in the temperature rise rate. Therefore, the end time of phase change in each group

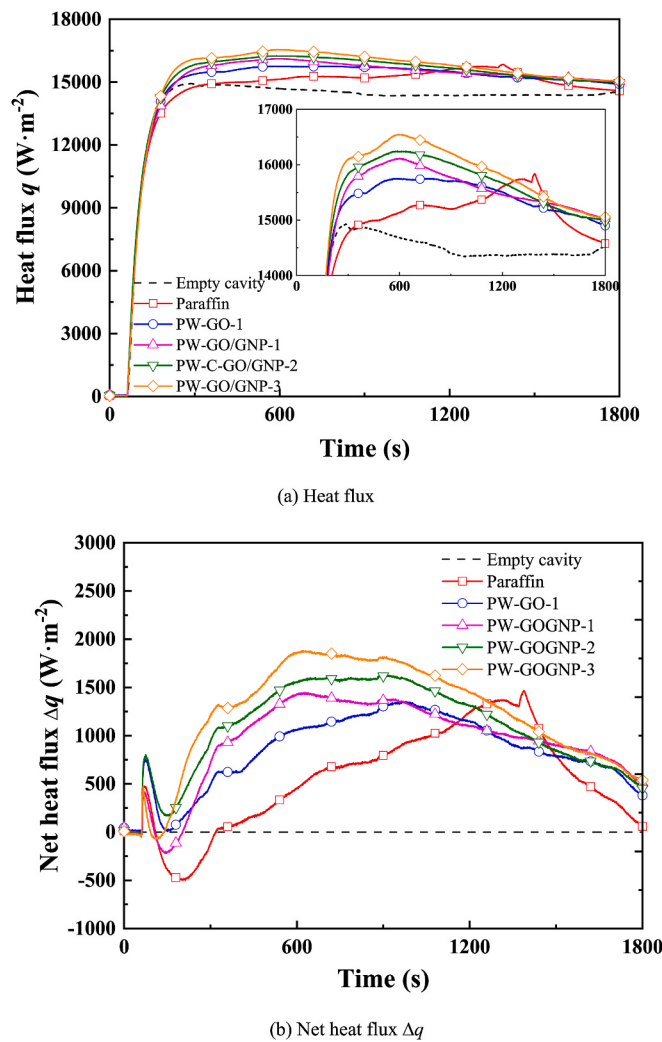


Fig. 7. Variations of heat flux and net heat flux through the heat conduction section in each experimental test.

can be determined by the peak value of the temperature increase rate. Similar to the paraffin group, the composite material group also had fluctuations in the temperature rise rate, as shown in Fig. 6(b). Based on the above paraffin analysis, it can be inferred that the phase transition end time of PW-GO-1, PW-GO/GNP-1 and PW-GO/GNP-2 are 225 s, 190 s and 21 s later than that of the paraffin group, respectively, and only that of the PW-GO/GNP-3 group is 98 s earlier. This indicates that the phase change process is simultaneously affected by internal heat conduction and convection. The convection suppression effect of graphene aerogels decreases the melting rate, which is harmful to the latent heat rapid release.

Based on the above discussions, the heat transfer process of CPCMs can be illustrated as three stages: first, pure heat conduction is the initial stage before the solid-liquid phase change starts, where the thermal conductivity coefficient is the main influencing factor, and the heat is

absorbed and converted into PCMs sensible heat. Second, with the phase change beginning, latent heat is activated to absorb heat and the molten paraffin starts to produce convection, after which internal convection and heat conduction combine to influence the phase change process. However, the composite material has opposite effects of heat conduction enhancement and convection suppression because the graphene aerogel inhibits the paraffin convection. Therefore, it is necessary to increase the thermal conductivity to a certain value to improve the thermal control effect and phase change rate of CPCMs in applications. Third, after the phase change, fluid convection and heat conduction decide the heat transfer in pure PCMs, but heat conduction is still dominant in CPCMs. In this stage, PCMs latent heat is fully utilized and the heat is converted into sensible heat, so the heat dissipation effect of the temperature control will be reduced.

3.1.2. Evaluation of heat dissipation enhancement of composite materials

The heat dissipation effect of the temperature control unit is affected by its heat conduction, convection and phase change. In order to further quantify the heat dissipation capability, the heat flux absorbed in PCMs is evaluated in this section.

As shown in Fig. 7(a), the heat flux variation of composite materials presented the same characteristic as the temperature variation without dramatic change. However, it is worth noting that the heat flux of composite material increases to the maximum within the first 600 s and then begins to decrease, which is significantly different from that of the paraffin group. The opposite effect between heat conduction enhancement and convective inhibition in composites is reflected again in the above heat flux characteristics. In the early stage, heat conduction dominated the heat transfer, so the heat dissipation of CPCMs had obvious advantages. The heat flux was higher than that of the paraffin cavity. However, the liquid paraffin increased as the phase change proceeded, and its natural convection strengthened the internal heat transfer, causing the heat flux of the paraffin group to rise gradually. In contrast, the heat flux of the composite material group started to decline due to convection inhibition. As a result, the heat flux of paraffin is higher than that of CPCMs at a certain period in the late heating stage, which means the heat dissipation of the paraffin group is better now.

Because the cavity is made of aluminum alloy except for the visible plexiglass, the heat flux can reach $15000 \text{ W}\cdot\text{m}^{-2}$ even cavity without PCMs. As shown in Fig. 7(b), the heat flux difference between the empty cavity and other groups with PCMs/CPCMs is calculated to eliminate the aluminum influence, which can be interpreted as the heat dissipation effect due to the addition of PCMs/CPCMs. There is a small increase and decrease in the initial stage of the net heat flux in Fig. 7(b), caused by the air convection inside the empty cavity. The net heat dissipation caused by PCMs/CPCMs in each group can be obtained as follows:

$$Q_n = \int_{60}^{1800} A \cdot \Delta q(t) dt \quad (2)$$

where A is the cross-sectional area (m^2), and Δq is the heat flux difference between the empty cavity group and other groups ($\text{W}\cdot\text{m}^{-2}$). According to the net heat dissipation of each group, the heat dissipation enhancement efficiency of CPCMs is defined as follows:

Table 4
Summary of heat dissipation enhancement efficiency for each unit.

Case	Curve integration / $\text{J}\cdot\text{m}^{-2}$	Contact intercept area/ m^2	Net heat dissipation /J	Graphene mass fraction	Enhanced efficiency
Pure paraffin	991009.7	0.0004	396.40	0%	100%
PW-GO-1	1508555.7		603.42	1.66%	152.2%
PW-GO/GNP-1	1683633.7		673.45	2.01%	169.9%
PW-GO/GNP-2	1946844.5		778.74	3.35%	196.5%
PW-GO/GNP-3	2187857.4		875.14	4.40%	220.8%

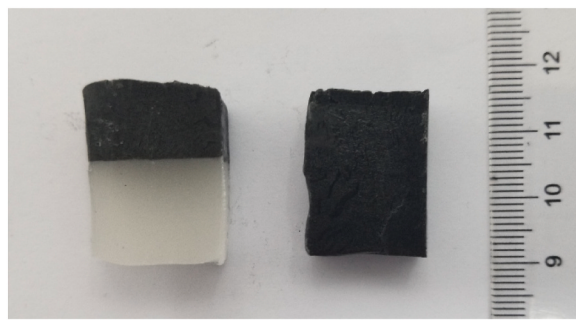


Fig. 8. Samples of different material combinations (left: paraffin combined with composite materials, right: a combination between different composite materials).

$$\eta = \frac{Q_{n-c}}{Q_{n-b}} \cdot 100\% \quad (3)$$

where Q_{n-c} and Q_{n-b} are the net heat dissipation of the composite material groups and paraffin group (J). As shown in Table 4, the heat dissipation enhancement efficiencies of composites PW-GO-1, PW-GO/GNP-1, PW-GO/GNP-2, and PW-GO/GNP-3 were 152.2%, 169.9%, 196.5%, and 220.8%, respectively.

3.2. Effect of PCM cascade arrangement on heat transfer performance

The effects of two PCM cascade arrangements on heat transfer performance are discussed in this section. Section 3.2.1 introduces the cascade method and arrangement layout. Sections 3.2.2 and 3.2.3 investigate the heat transfer of the longitudinal and horizontal cascade arrangements.

3.2.1. PCM cascade arrangement layout

Paraffin will soften at a temperature slightly below the phase change melting point. In the softened state, it is easier to cut and form a smooth

cut surface, making it can be combined and compacted in the mold. Therefore, the non-uniform arrangement of physical properties in a single cavity can be achieved through splicing PCM blocks with different physical properties, thus, the local regulation of the heat transfer process can be performed as shown in Fig. 8. Two different cascade arrangements are performed in this section to coordinate the internal heat transfer, convection and phase change processes of the temperature control unit.

Longitudinal cascade arrangement: The prepared composite material block, 2.21 g each of PW-GO/GNP-1, PW-GO/GNP-2, and PW-GO/GNP-3, was placed in a single cavity in turn. After heating at low power and keeping the temperature below 48 °C to soften the composite material, a square wood was used to apply pressure to the cavity. In this way, the cascade arrangement and splicing of the three composite materials can be achieved. The cascade combinations are named G-PCC-1 and G-PCC-2, with material distributions shown in Fig. 9. The longitudinal cascade arrangement can fully utilize the high thermal conductivity of graphene CPCMs.

Horizontal cascade arrangement: The composite material PW-GO/GNP-3 with a mass of 3.012 g was cut and placed in the cavity center, as shown in Fig. 10. Then, the space on the left and right sides was filled with pure paraffin until the total mass of the phase change material in the cavity reached 6.63 g. This horizontal cascade combination is named C-PCC. The porous content of the 6.63 g PW-GO/GNP-1 in the single cavity was 0.1333 g. According to the mass fraction of PW-GO/GNP-3 (4.40%), the porous material content of C-PCC was 0.1325 g, which is equivalent to concentrating the composite porous material of the same mass in a local area. The horizontal cascade arrangement aims to combine heat conduction enhancement and convection.

3.2.2. Heat transfer of the longitudinal cascade arrangement

The experimental conditions and methods were consistent with those of the above experiments. As shown in Fig. 11, the net heat dissipation of PW-GO/GNP-2, G-PCC-1 and G-PCC-2 is 778.74 J, 688.12 J and 822.61 J. The arrangement with the highest net heat dissipation is G-PCC-2, i.e., the longitudinal cascade arrangement in which PW-GO/GNP-3 with

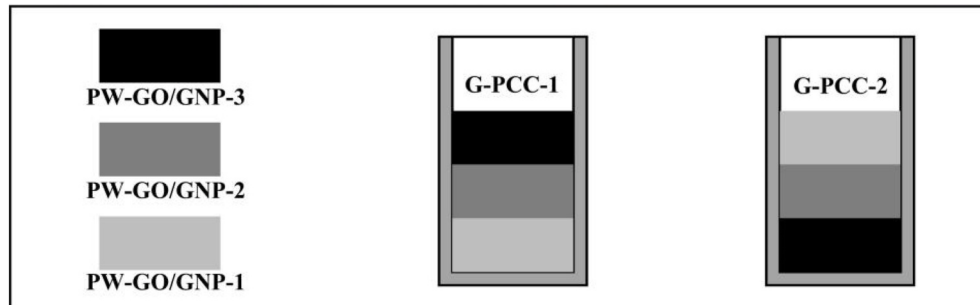


Fig. 9. Schematic arrangement of CPCMs longitudinal cascade in the cavity.

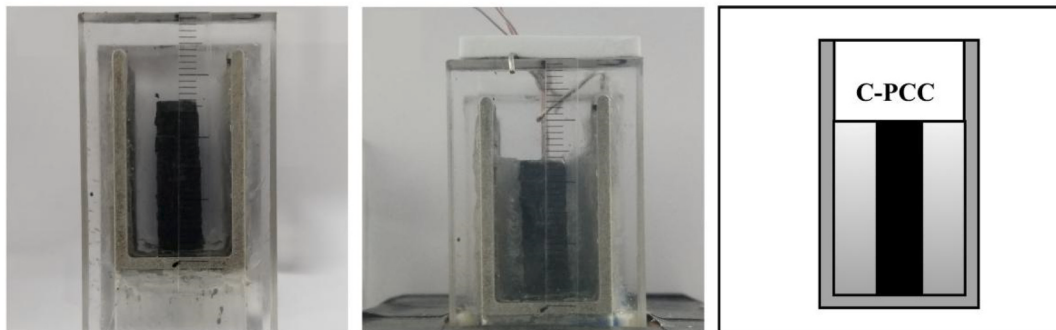


Fig. 10. Schematic of PCMs horizontal mixing arrangement in the cavity.

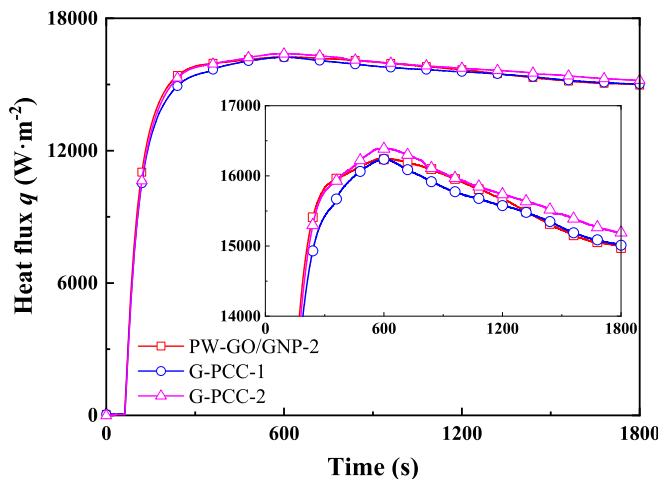
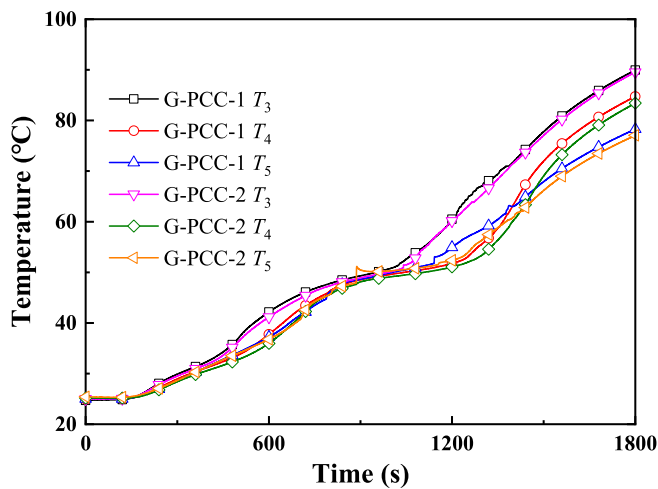
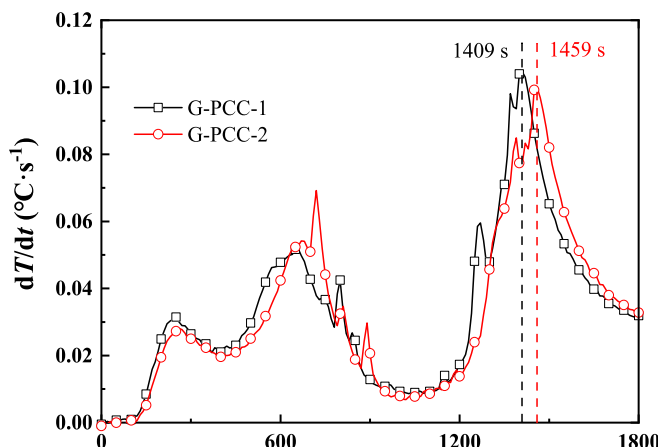


Fig. 11. Net heat flux of longitudinal thermal conductivity cascade arrangement groups.



(a) Internal temperature (T_3 , T_4 and T_5)



(b) Center temperature (T_4) variation rate

Fig. 12. Internal temperature and temperature variation rate of T_4 in longitudinal thermal conductivity cascade arrangements.

high thermal conductivity is used at the bottom and PW-GO/GNP-1 with low thermal conductivity is used at the top. Compared with pure paraffin, the enhanced heat dissipation efficiency of G-PCC-2 is 207.5%, which is 11% higher than that of the pure PW-GO/GNP-2 group. G-PCC-1 has the lowest net heat dissipation, with an enhanced heat dissipation efficiency of only 173.6%. Therefore, it can be concluded that a reasonable longitudinal stepped arrangement can improve the temperature control effect more than a uniform arrangement in a single cavity. The heat dissipation effect is best when the thermal conductivity increases from top to bottom.

The temperature variations of the internal Locations inside the cascade arrangement group are shown in Fig. 12(a). At Location 3, the temperature changes of G-PCC-1 and G-PCC-2 are quite close. While at Locations 4 and 5, the temperature of G-PCC-2 keeps lower than that of G-PCC-1. The temperature increase rate of T_4 is presented in Fig. 12(b). It can be seen that the phase transition end time of G-PCC-1 and G-PCC-2 are at $t = 1409$ s and 1459 s, respectively. Although the phase transition time required for G-PCC-2 is slightly higher, its contribution to heat conduction optimization is greater, resulting in a better heat dissipation effect.

3.2.3. Heat transfer of the horizontal cascade arrangement

According to the analysis of section 3.1, graphene aerogel has the opposite effects of heat conduction enhancement and convection suppression, while its advantage of high thermal conductivity is only reflected in the initial heating stage. Therefore, there is still much room for heat dissipation improvement by controlling convective heat transfer in CPCMs. The horizontal cascade arrangement (C-PCC) was designed as a combination of heat conduction and convection enhancement in this section. Fig. 13 shows some photos of the C-PCC group during the experiment. It can be seen that the phase transition rate of paraffin in the cascade arrangement is much faster than that of the pure paraffin group. The phase transition started to advance inward near the two sidewalls, forming a fish-shaped region ($t = 960$ s) with a wide top and a narrow bottom due to the presence of composite material in the middle region, which is opposite of the narrow top and wide bottom in the pure paraffin group [30]. The upward convection in the pure paraffin area on both sides formed a recirculation area to advance the phase change interface, while the bottom had not only local natural convection but also local heat conduction enhancement of the composite material, making the lower phase interface advance faster than the upper one.

The heat flux variation of the horizontal arrangement group with time is shown in Fig. 14(a). It can be seen that the heat flux of the combination arrangement combined the characteristics of the composite material and the pure paraffin, with a peak in the early and late stages, and was higher than that of the pure paraffin. Therefore, the horizontal cascade arrangement achieved the effective combination of heat conduction enhancement and convection heat transfer, where the heat conduction enhancement dominated in the early stage, and the convective heat transfer maintained the high heat flux in the middle and late stages. The net heat flux, excluding the heat flux of the empty cavity, is shown in Fig. 14(b). It can be seen that the heat flux of the combined arrangement group is lower than that of the other two composite groups but higher than that of the paraffin group in the early heating stage because its near-wall areas on both sides are paraffin. As the subsequent melting and convection progressed, the heat flux of the combined arrangement group began to overtake, surpassing that of composite PW-GO/GNP-1 and PW-GO/GNP-2 groups at $t = 836$ s and 1054 s.

Furthermore, the instantaneous comparison images of the test group at those two intersection points are attached in Fig. 14(b). In the combined arrangement group, the paraffin near the wall had started to melt at $t = 836$ s, forming a bilateral symmetrical convection area. At $t = 1054$ s, the paraffin in the combined arrangement group finished melting and the convection space was getting larger, leaving only a little paraffin remaining in the central region. However, significant convection could not be observed in the pure CPCMs groups. As a result, the net

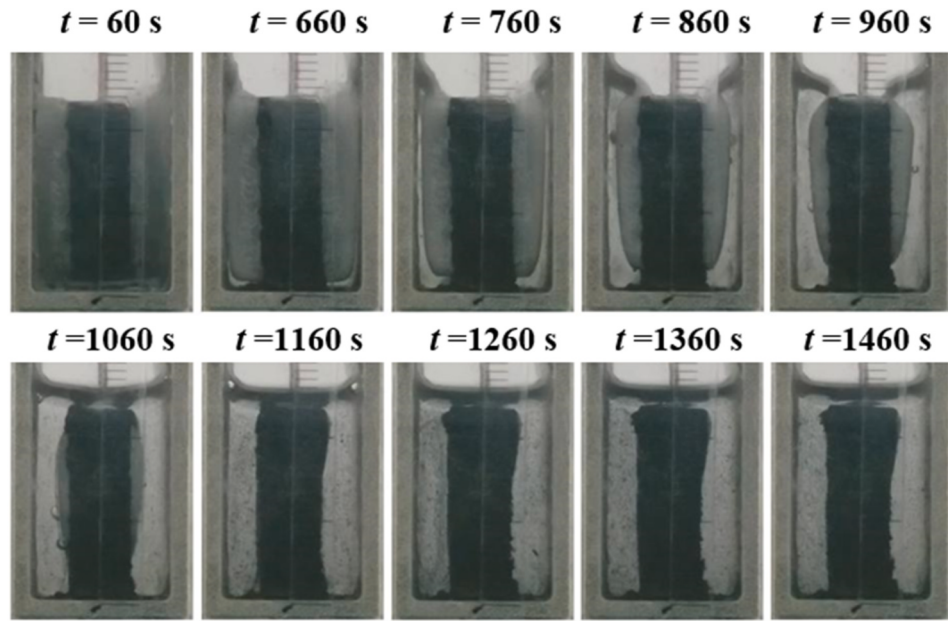
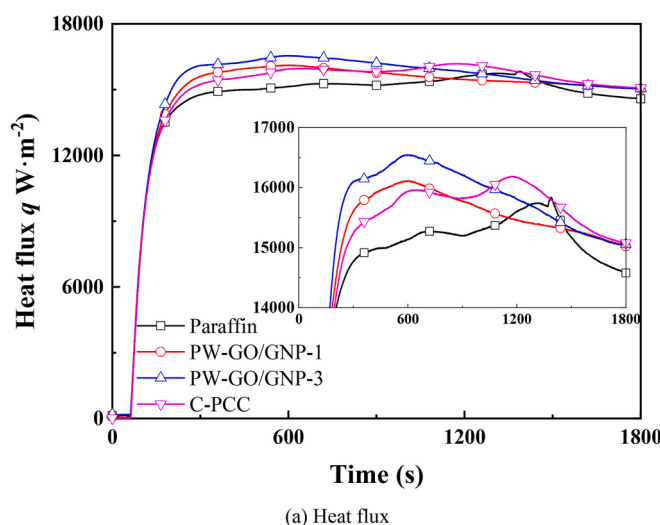
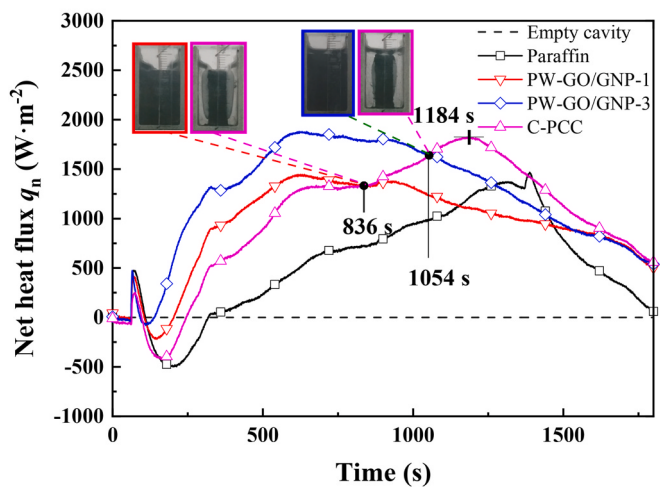


Fig. 13. Photos of the melting process in the horizontal mixed group.



(a) Heat flux



(b) Net heat flux

Fig. 14. Heat flux and net heat flux of horizontal mixing arrangement group and composite groups.

heat flux of the combined arrangement group gradually exceeded that of the pure PCMs groups. Besides, the net heat dissipation capacity of the combined arrangement group was 720.98 J, and the enhanced heat dissipation efficiency was 181.9%. Therefore, using the same amount of porous materials, the heat dissipation of the combined arrangement is 12% more effective than that of the group filled with pure PW-GO/GNP-1 composite.

The temperature variation of internal Locations 3–5 in the combined arrangement group is shown in Fig. 15(a). It can be seen that T_3 , T_4 and T_5 are very close in the horizontal cascade group, which means the longitudinal temperature difference in the cavity was small. Moreover, T_5 is higher than T_4 before 1423 s due to the convection effect of the pure paraffin area on both sides. As shown in Fig. 15(b), the temperature rise rate of Location 4 peaked at $t = 1411$ s, so the phase transition end time of the test unit is 1411 s. Compared with the 1560 s of the composite PW-GO/GNP-1 group, the phase change speed was increased by 149 s. Therefore, the combination arrangement proposed in this section can enhance the heat transfer and promote the melting rate.

4. Conclusions

A visual phase change experimental test platform was established to investigate the heat transfer characteristics of graphene aerogel CPCMs in this study. Moreover, the effects of PCM cascade arrangement on heat transfer performance are discussed in detail. The main conclusions are drawn as follows:

- Four graphene aerogel CPCMs with high thermal conductivity were prepared using the hydrothermal self-assembly method, and using graphene CPCMs can improve thermal control. The maximum heat dissipation enhancement efficiency of those CPCMs can reach 220.8%.
- Unlike pure paraffin, heat conduction dominates the heat transfer in CPCMs after phase transition. Graphene aerogel has opposite effects of heat conduction enhancement and convection suppression, decreasing the melting rate. However, improving the thermal conductivity of CPCMs can reduce the convection inhibition effect.
- PCMs combination with different physical properties can be performed through splicing and shaping. Two novel cascade arrangements are proposed to coordinate the internal heat transfer,

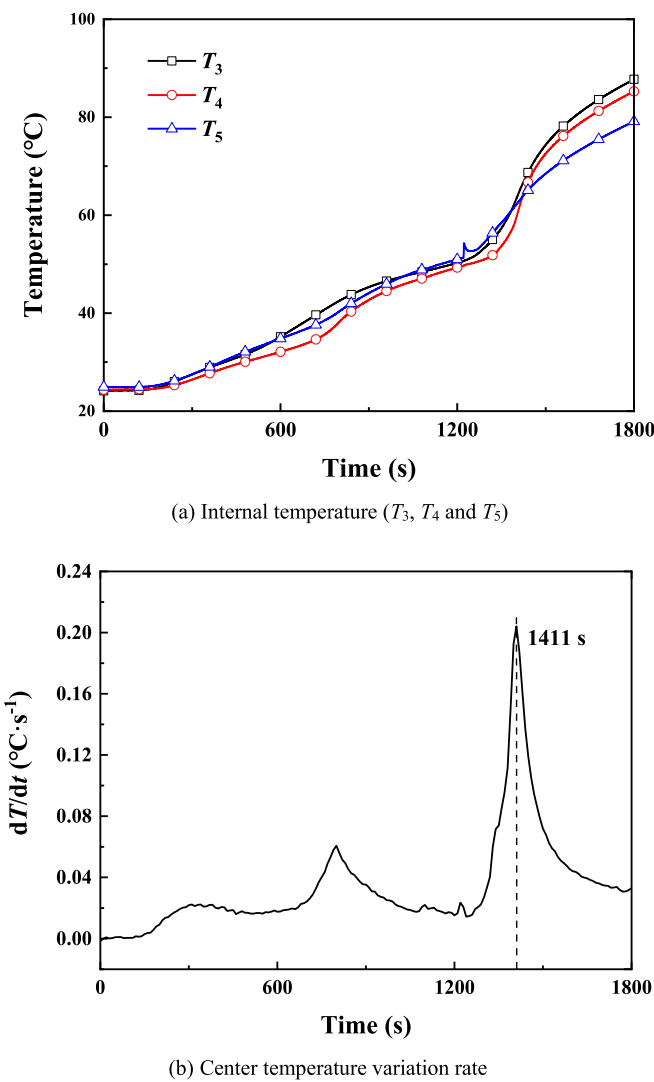


Fig. 15. Internal temperature and temperature variation rate of T_4 in horizontal mixing arrangement.

- convection and phase change processes of PCMs. Longitudinal thermal conductivity cascade arrangements improve temperature control more than a uniform arrangement. The effect is best when the thermal conductivity increases from top to bottom (G-PCC-2). The enhanced heat dissipation efficiency of G-PCC-2 is 207.5%, which is 11% higher than that of the pure PW-GO/GNP-2 group.
4. Graphene aerogel CPCMs have high thermal conductivity, while there is much room for heat dissipation improvement by controlling convective heat transfer in graphene CPCMs. The horizontal cascade arrangement proposed in this study effectively combines heat conduction enhancement and convection heat transfer, which can enhance heat transfer and promote the melting rate. Heat dissipation is 12% more effective than the cavity filled with pure PCMCs using the same amount of porous materials. The phase change speed was increased by 149 s compared with the composite PW-GO/GNP-1 group.

Conclusions obtained from this work illuminate heat transfer and phase change characteristics of graphene aerogel CPCMs, which paves the application foundation for the thermal management of graphene CPCMs. For example, graphene aerogel has the opposite effects of heat conduction enhancement and convection suppression, but improving the thermal conductivity of CPCMs can reduce the convection inhibition

effect. Therefore, it is necessary to increase the thermal conductivity to a certain value (at least 209.7% enhancement in this study) to improve the thermal control effect and phase change rate of CPCMs in applications, which also can be used to guide CPCMs preparation. Moreover, new cascade arrangements designed in this study provide new ideas on heat transfer improvement.

However, the effects of cascade number and pure paraffin content on two cascade arrangements are not discussed in this study. For the wide application of graphene CPCMs, predictions of the optimal graphene ratio in preparation and the best cascade parameters in applications will be investigated using machine learning and big data analysis in our future work.

Declaration of competing interest

We declare that there is no conflict of interest exists in the submission of this manuscript, as well as the manuscript is approved by all authors for publication. I would like to declare on behalf of my co-authors that work described was original research that has not been published previously, and not under consideration for publication elsewhere, in whole or in part.

Data availability

Data will be made available on request.

Acknowledgements

We would like to acknowledge financial supports for this work provided by the National Natural Science Foundation of China (No.52176085, No.52276083).

References

- [1] He ZQ, Yan YF, Zhang ZE. Thermal management and temperature uniformity enhancement of electronic devices by micro heat sinks: a review. Energy 2021;216.
- [2] Cheng WL, Liu N, Wu WF. Studies on thermal properties and thermal control effectiveness of a new shape-stabilized phase change material with high thermal conductivity. Appl Therm Eng 2012;36:345–52.
- [3] Kahwaji S, Johnson MB, Kheirabadi AC, Groulx D, White MA. A comprehensive study of properties of paraffin phase change materials for solar thermal energy storage and thermal management applications. Energy 2018;162:1169–82.
- [4] Tong X, Li NQ, Zeng M, Wang QW. Organic phase change materials confined in carbon-based materials for thermal properties enhancement: recent advancement and challenges. Renewable Sustainable Energy Rev 2019;108:398–422.
- [5] Ibrahim NI, Al-Sulaiman FA, Rahman S, Yilbas BS, Sahin AZ. Heat transfer enhancement of phase change materials for thermal energy storage applications: a critical review. Renewable Sustainable Energy Rev 2017;74:26–50.
- [6] Krzywanski J, Grabowska K, Sosnowski M, Zylka A, Kulakowska A, Czakiert T, et al. Heat transfer in adsorption chillers with fluidized beds of silica gel, zeolite, and carbon nanotubes. Heat Tran Eng 2022;43(3–5):172–82.
- [7] Grabowska K, Sztekler K, Krzywanski J, Sosnowski M, Stefanski S, Nowak W. Construction of an innovative adsorbent bed configuration in the adsorption chiller part 2. experimental research of coated bed samples. Energy 2021;215:119123.
- [8] Pizzolato A, Sharma A, Maute K, Sciacovelli A, Verda V. Design of effective fins for fast PCM melting and solidification in shell-and-tube latent heat thermal energy storage through topology optimization. Appl Energy 2017;208:210–27.
- [9] Mahdi JM, Nsofor EC. Solidification enhancement in a triplex-tube latent heat energy storage system using nanoparticles-metal foam combination. Energy 2017;126:501–12.
- [10] Li JY, Hu XW, Zhang C, Luo WX, Jiang XX. Enhanced thermal performance of phase-change materials supported by mesoporous silica modified with polydopamine/nano-metal particles for thermal energy storage. Renew Energy 2021;178:118–27.
- [11] Alvar MZ, Abdeali G, Bahramian AR. Influence of graphite nano powder on ethylene propylene diene monomer/paraffin wax phase change material composite: shape stability and thermal applications. J Energy Storage 2022;52.
- [12] Li M, Guo QG, Su YL. The thermal conductivity improvements of phase change materials using modified carbon nanotubes. Diam Relat Mater 2022;125.
- [13] Gao HY, Wang JJ, Chen X, Wang G, Huang XB, Li A, et al. Nanoconfinement effects on thermal properties of nanoporous shape-stabilized composite PCMs: a review. Nano Energy 2018;53:769–97.
- [14] Shang Y, Zhang D. Preparation and characterization of three-dimensional graphene network encapsulating 1-hexadecanol composite. Appl Therm Eng 2017;111:353–7.

- [15] Liao HH, Chen WH, Liu Y, Wang Q. A phase change material encapsulated in a mechanically strong graphene aerogel with high thermal conductivity and excellent shape stability. *Compos Sci Technol* 2020;189.
- [16] Wu YP, Zhu JH, Huang L. A review of three-dimensional graphene-based materials: synthesis and applications to energy conversion/storage and environment. *Carbon* 2019;143:610–40.
- [17] Bai J, Zhang B, Yang BL, Shang JX, Wu ZQ. Preparation of three-dimensional interconnected graphene/ionic liquid composites to enhanced thermal conductivities for battery thermal management. *J Clean Prod* 2022;370.
- [18] Wang H, Zhang Y, Ci ED, Li XQ, Li JQ. An experimental study in full spectra of solar-driven magnesium nitrate hexahydrate/graphene composite phase change materials for solar thermal storage applications. *J Energy Storage* 2021;38.
- [19] Luo RR, Lei H, Shao FL, Wang LL, Xie HQ, Yu W. Graphene-pentaerythritol solid-solid phase change composites with high photothermal conversion and thermal conductivity. *Sol Energy* 2022;241:54–62.
- [20] Sathishkumar A, Cheralathan M. Charging and discharging processes of low capacity nano-PCM based cool thermal energy storage system: an experimental study. *Energy* 2023;263.
- [21] Arici M, Bilgin F, Nižetić S, Karabay H. PCM integrated to external building walls: an optimization study on maximum activation of latent heat. *Appl Therm Eng* 2020;165:114560.
- [22] Zhang LJ, Yang P, Li W, Klemes JJ, Zeng M, Wang QW. A new structure of PCHE with embedded PCM for attenuating temperature fluctuations and its performance analysis. *Energy* 2022;254.
- [23] Chen MY, Cui YL, Ouyang DX, Weng JW, Liu JH, Zhao LY, et al. Experimental study on the hybrid carbon based phase change materials for thermal management performance of lithium-ion battery module. *Int J Energy Res* 2022;46(12):17247–61.
- [24] Park J, Choi SH, Karng SW. Cascaded latent thermal energy storage using a charging control method. *Energy* 2021;215.
- [25] Wang M, Wang Y, Zhang C, Yu FQ. Cascade phase change based on hydrate salt/carbon hybrid aerogel for intelligent battery thermal management. *J Energy Storage* 2022;45.
- [26] ELSihy ES, Xu C, Du XZ. Cyclic performance of cascaded latent heat thermocline energy storage systems for high-temperature applications. *Energy* 2022;239.
- [27] Christopher S, Parham K, Mosaffa AH, Farid MM, Ma ZJ, Thakur AK, et al. A critical review on phase change material energy storage systems with cascaded configurations. *J Clean Prod* 2021;283.
- [28] Tong X, Zhang LJ, Zeng M, Wang QW. Experimental investigation on preparation and characterization of paraffin/graphene aerogel. *J Eng Thermophys* 2020;41(10):2518–23.
- [29] Hu H, Zhao ZB, Wan WB, Gogotsi Y, Qiu JS. Ultralight and highly compressible graphene aerogels. *Adv Mater* 2013;25(15):2219–23.
- [30] Yang P, Tong X, Zeng M, Wang Q. Numerical investigation on temperature control characteristics based on phase change temperature gradient arrangement. *J Eng Thermophys* 2022;43(6):1625–30.